Arch. Metall. Mater. **71** (2026), 2, 561-564

DOI: https://doi.org/10.24425/amm.2026.158841

JUNGMIN JEON[1], SEONGHYUN PARK[1], EUNJOO SHIN[2], JAE-WON LIM[1,3], JAE-GIL JUNG[1,3*]

MICROSTRUCTURE AND MECHANICAL PROPERTIES OF P-MODIFIED Al–25Mg_2Si–6Mg–11Cu–11Zn ALLOY

We study the microstructure and precipitation behavior of P-modified Al–25Mg_2Si alloy with excess Mg, Cu, and Zn. The addition of P significantly refines the primary Mg_2Si phase (from 165 to 43 μm) due to enhanced heterogeneous nucleation at the Mg_3P_2 phase. This refinement leads to improvements in compressive strength (from 440 to 585 MPa) and fracture strain (from 3.0 to 3.6%). The solution-treated alloy containing partially spheroidized and smoothed secondary phases exhibits significant age hardening at both 25°C and 120°C. Transmission electron microscopy (TEM) and small-angle neutron scattering (SANS) analyses confirm the formation of Guinier-Preston (GP) zones, η', and η nanoprecipitates during aging at 120°C. Solution and subsequent peak-aging enhance the compressive strength (from 585 to 722 MPa) and fracture strain (from 3.6 to 4.0%) of the alloy.

Keywords: Aluminum alloys; microstructure; precipitation; transmission electron microscopy; small-angle neutron scattering

1. Introduction

Al–Mg_2Si alloys have attracted considerable interest for lightweight structural applications owing to their low density and high hardness [1]. Hard Mg_2Si phases often deteriorate the mechanical properties due to their coarse dendritic morphologies [2], acting as the sites for stress concentration [3,4]. To overcome these limitations, various alloying strategies (e.g., P [5], Y/Sb [6], Ti [7], and Cu [8]) have been developed to refine or modify the Mg_2Si phases and improve mechanical properties.

The additions of precipitate-forming elements have also been used to improve the mechanical properties of Al–Mg_2Si alloys [9-12]. Li et al. [9] reported that the addition of Cu and Zn to Al–5Mg–2Si (wt.%) alloy (Al–7Mg_2Si) induces the precipitation of T-$Mg_{32}(AlCuZn)_{49}$ and S-Al_2CuMg phases during aging, thus improving the alloy strength. Baek et al. [10] reported that the addition of Cu and Zn induces the formation of Zn/Cu-rich solute clusters during natural aging of Al–7Mg–9Si–10Cu–10Zn (wt.%) alloy (Al–11Mg_2Si). Recently, the present authors found that a highly-alloyed Al–22Mg–9Si–11Cu–11Zn (wt.%) alloy (Al–25Mg_2Si) with coarse dendritic Mg_2Si phases exhibits a significant age hardening due to η-$Mg(Zn,Cu,Al)_2$ precipitation [13]. In this study, follow-up studies were conducted to investigate the synergistic effect of P modification and precipitation strengthening on the mechanical properties of P-added Al–25Mg_2Si alloy with excess Mg, Cu, and Zn.

2. Experimental

High-purity metals (Al, Mg, and Zn) and master alloys (Al–50Cu, Al–25Si, and Al–5P) were melted at 850°C in an induction-melting furnace with a protective gas (SF_6:CO_2 = 1:10) to prevent oxidation. 1.5 kg of P-added Al–25Mg_2Si–6Mg–11Cu–11Zn (wt.%) alloy melt was degassed using Ar gas bubbling filtration and cast into a copper book mold (240×200×70 mm^3) preheated to ~140°C. The P concentration of the ingot was measured to be 0.006 wt.%. A 22 g of the alloy ingot was remelted at 830°C using a vacuum induction melting (BLUE POWER MC20V) and cast into a Cu mold (Φ12×60 mm) preheated to 200°C. As-cast ingots were solution-treated at 450°C for 1 h and 24 h and then quenched into water. The solution-treated alloy for 24 h was immediately aged at 25°C and 120°C, followed by water-quenching.

After the specimens (Φ12×1 mm) were mechanically polished, the microstructure was examined using scanning electron microscopy (SEM, Hitachi, SU3900) and energy dispersive X-ray spectroscopy (EDS). The precipitates were investigated using transmission electron microscopy (TEM, FEI, Talos F200X G2) and EDS installed at the Center for University-wide Research Facilities (CURF) at Jeonbuk National University. TEM samples were prepared by the focused ion beam (FIB) technique.

To investigate age hardening behavior, the Vickers hardness of the Al matrix was measured under a load of 50 g with a dwell

[1] JEONBUK NATIONAL UNIVERSITY, DIVISION OF ADVANCED MATERIALS ENGINEERING, JEONJU 54896, REPUBLIC OF KOREA
[2] KOREA ATOMIC ENERGY RESEARCH INSTITUTE (KAERI), NEUTRON SCIENCE DIVISION, DAEJEON
[3] JEONBUK NATIONAL UNIVERSITY, RESEARCH CENTER FOR ADVANCED MATERIALS DEVELOPMENT, JEONJU 54896, REPUBLIC OF KOREA

* Corresponding author: jgjung@jbnu.ac.kr

time of 10 s using a Vickers hardness tester (TIME TH715). Electrical conductivity was measured using Fischer Technology SIGMASCOPE SMP-350. Compression tests of cylindrical specimens (Φ4×6 mm) were performed using a universal testing machine (Instron, Model 5569) at a strain rate of 1×10^{-3} s^{-1}.

Small-angle neutron scattering (SANS) measurements were carried out using the 18M-SANS instrument at HANARO in the Korean Atomic Energy Research Institute (KAERI) with cylindrical specimens (Φ10×0.6 mm). Neutron beams with wavelengths of 5 Å and 10 Å were employed, and the sample-to-detector distances were set to 3.1 m and 9.1 m, respectively. The obtained 2D nuclear scattering patterns were converted into 1D data using Igor Pro9 software (NIST) [14], and fitting of the 1D data was performed using the SASfit software [15].

3. Results and discussion

Fig. 1(a) shows an SEM image of an as-cast alloy consisting of dendritic primary Mg_2Si, S-Al_2CuMg, and Al/η-$Mg(Zn,Cu,Al)_2$ eutectic. The length and areal number density of the primary Mg_2Si phase were measured to be 43±21 μm and 274±51 mm^{-2}, which were smaller and denser than those of the P-free alloy (165±51 μm and 103±24 mm^{-2}) [13]. Fig. 1(b) shows that the P-containing particles exist within the primary Mg_2Si phase of the P-added alloy ingot used for remelting. These P-containing phases correspond to the thermally stable Mg_3P_2 phase above 800°C, as calculated using FactSage software (not provided). The Mg_3P_2 phase, formed before the primary Mg_2Si phase (~750°C), served as a heterogeneous nucleation site for the primary Mg_2Si phase, thereby leading to P-induced Mg_2Si phase refinement [16]. Figs. 1(c,d) show SEM images of solution-treated alloys for 1 and 24 h, respectively. This indicates that the sharp interface of the primary Mg_2Si phase was partially smoothed, and the η and S phases were spheroidized by solution treatment.

Fig. 2(a) shows the evolution of microhardness and electrical conductivity during aging at 25 and 120°C. Natural aging at 25°C for 10000 h resulted in a gradual increase in microhardness (from 107 to 187 HV) and a decrease in electrical conductivity (from 5.2 to 4.8 MS/m). Meanwhile, after artificial aging at 120°C, the microhardness rapidly increased to 204 HV in 1 h and then gradually increased to the maximum of 215 HV over 8 h. After overaging for 1000 h, the microhardness was reduced to 173 HV, and the electrical conductivity increased to 6.5 MS/m.

Fig. 2(c) shows TEM results of the overaged alloy at 120°C for 1000 h. There are elongated precipitates (~50 nm) that exist along low-angle grain boundaries (LAGB) and S phase boundaries and Mg/Zn/Cu-rich nanoprecipitates (3.6±2.7 nm) in the Al matrix. High-resolution TEM (HRTEM) and fast Fourier transform (FFT) analyses reveal that nanoprecipitates are composed of η' and η precipitates having the orientation relationships of $[1010]_{\eta}\|[112]_{Al}$ [17] and $[21\text{–}1\text{–}0]_{\eta'}\|[112]_{Al}$ [18]. In addition, fine nanoprecipitates (<2 nm) were also found in the 1000 h-aged alloy.

Fig. 3(c) shows HRTEM and FFT results of the alloy aged at 120°C for 1 h, which corresponds to a nearly peak-aged condition. The η' precipitates are present along the interface of η phases, which are identified by 1/3 diffraction spots along the $\{111\}_{Al}$ planes [19]. This suggests the sequential formation of heterogeneously nucleated precipitates from η' (1 h) to η (1000 h). The Al

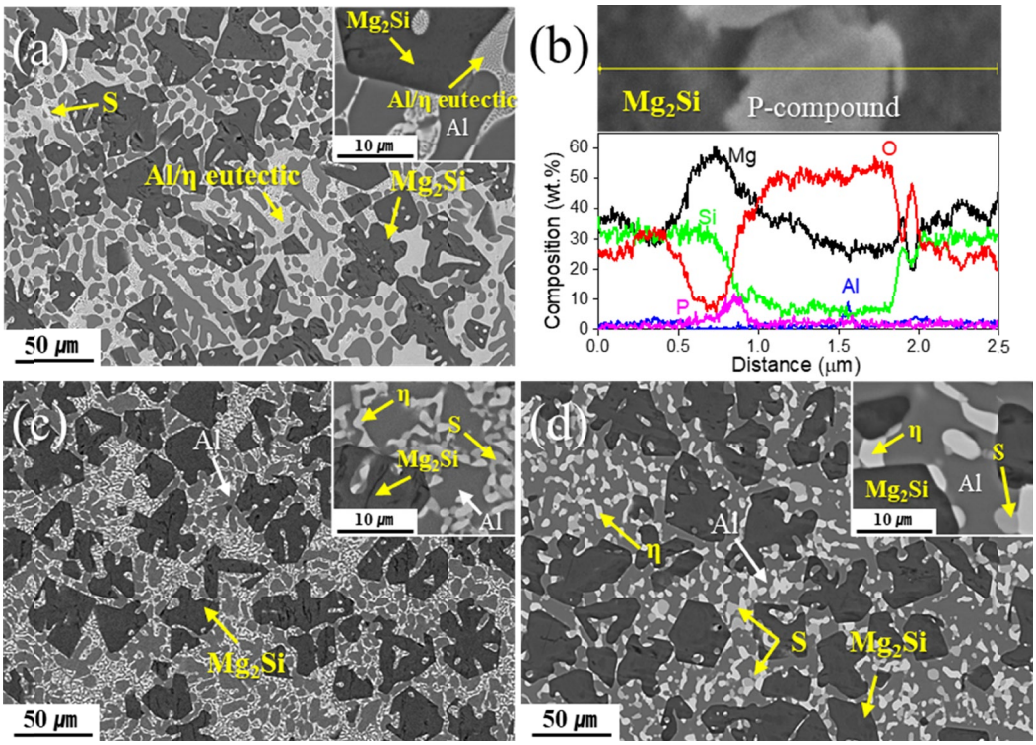

Fig. 1. (a) SEM image of as-cast alloy and (b) EDS result of P-compound located at the center of Mg_2Si phase. SEM image of solution-treated alloys for (c) 1 h and (d) 24 h

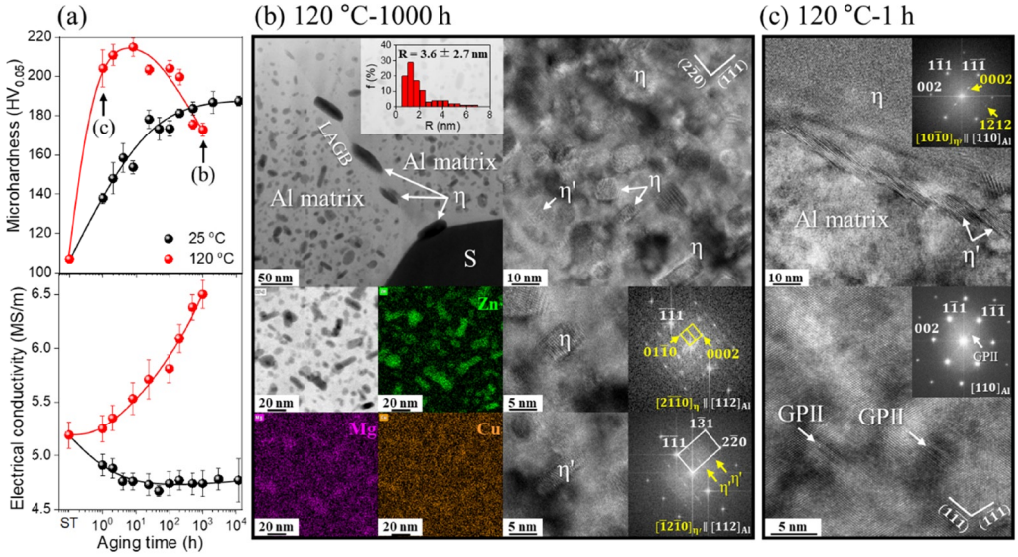

Fig. 2. (a) Evolution of microhardness and electrical conductivity during aging at 25°C and 120°C. TEM analysis of the alloys aged at 120°C for (b) 1000 h and (c) 1 h

matrix contains fine (<5 nm) coherent Guinier-Preston (GP) II zones that produce streaks $\{111\}_{Al}$ planes in the FFT pattern [20].

Fig. 3 shows the SANS curves of the alloys aged at 25°C and 120°C. For the alloy aged at 25°C for 3000 h (Fig. 3(a)), an increase in scattering intensity is observed in the high-Q region (>0.1 $Å^{-1}$), indicating the presence of very fine (~1 nm) nano-precipitates (~1 nm), which could not be analyzed in this study. The alloy aged at 120°C for 1 h (Fig. 3(b)) also shows an increase in scattering intensity in the high-Q region (>0.07 $Å^{-1}$). As the aging time at 120°C increases, the enhanced scattering region shifts to the lower Q region (Fig. 3(c,d)). The size distribution curves of the nanoprecipitates were obtained by fitting the SANS curves assuming a spherical shape and a difference in scattering length density values of 0.666×10^{-6} $Å^{-2}$ for the GP zones and 1.399×10^{-6} $Å^{-2}$ for the η precipitates [13].

The quantitative SANS analysis indicates that the 1 h-aged alloy at 120°C contains GP zones with an average radius of 0.98 nm and a volume fraction of 1.58%, which contribute to an increase in microhardness (204 HV) by the dislocation shearing mechanism [13]. The 8 h-aged alloy contains the GP zones with larger sizes (1.13 nm) and increased volume fraction (2.75%). This indicates the occurrence of growth of GPII zones, which leads to a further increase in microhardness (215 HV) due to the enhanced precipitation strengthening effect of dislocation-shearable GP zones. The contribution to precipitation strengthening can be estimated by applying the SANS data and the lattice misfit of the GP region

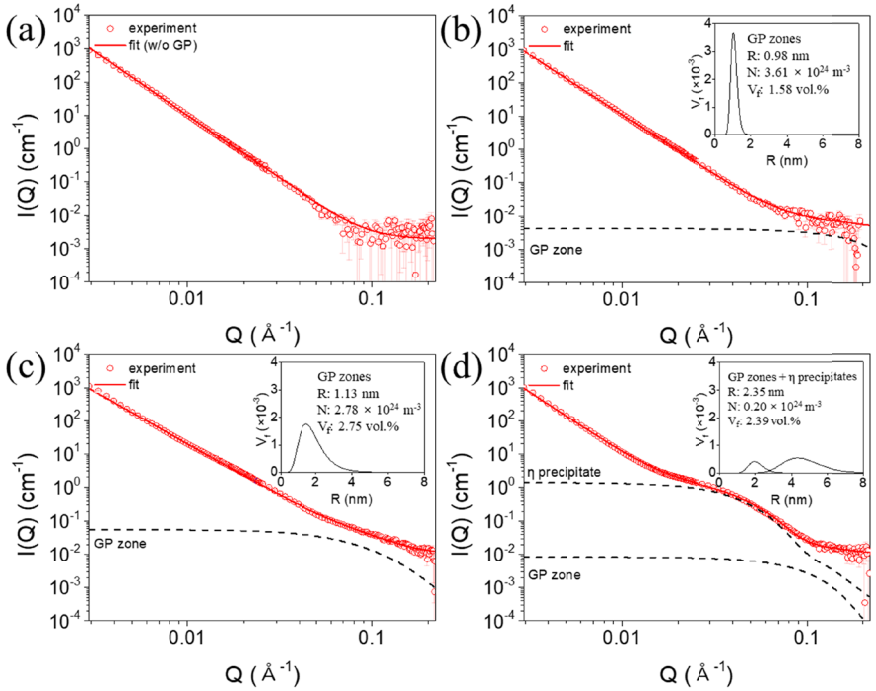

Fig. 3. SANS curves of the alloys aged at (a) 25°C for 3000 h and at 120°C for (b) 1 h, (c) 8 h, and (d) 1000 h (inset: precipitation size distribution)

(2.23% [13]) to the dislocation shear model [21]. The calculated contribution to precipitation strengthening corresponds to ~404 MPa, which is similar to the estimated yield strength (352 MPa) obtained through the microhardness increment (~108 HV) and the three times rule between them. The overaged alloy for 1000 h shows a bimodal size distribution of fine precipitates (GP zones) and coarse precipitates (η), with the average radius of 2.35 nm and volume fraction 2.39%. The coarsening of dislocation bypass precipitates reduced the strengthening effect [22], thereby lowering the microhardness (173 HV) of the overaged alloy.

Fig. 4 shows compressive stress-strain curves of as-cast and peak-aged alloys. The addition of P improved the maximum compressive strength (from 440±30 to 585±2 MPa) and fracture strain (from 3.0±0.2 to 3.6±0.1%) of as-cast alloys. These improvements are primarily due to the refinement of the primary Mg_2Si phase, which delays premature failure. Solution treatment and peak aging improved the compressive strength (722±26 MPa) and fracture strain (4.0±0.4%) of the P-added alloy, due to delayed failure (by spheroidization of secondary phases) and precipitation strengthening. This study provides insights into strategies for tailoring the microstructure to improve the mechanical performance of the highly alloyed Al–Mg_2Si system.

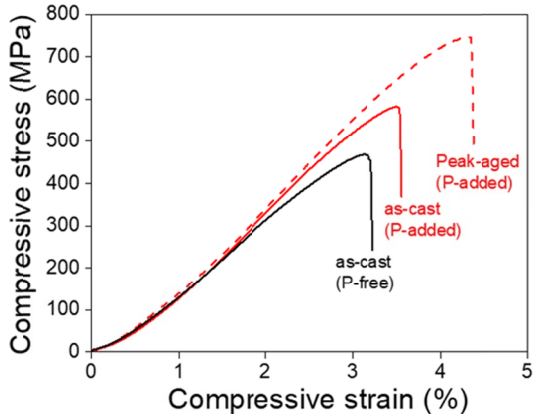

Fig. 4. Compressive stress-strain curves of the as-cast and peak-aged alloys with and without P addition

4. Conclusions

1. P-added Al–25Mg_2Si–6Mg–11Cu–11Zn alloy consisted of primary Mg_2Si, S-Al_2CuMg, and Al/η-$Mg(Zn,Cu,Al)_2$ eutectic, which were partially spheroidized by solution treatment at 450°C. The addition of P refined the primary Mg_2Si phase due to improved heterogeneous nucleation at the Mg_3P_2 particles.
2. Aging at 25 and 120°C increased the microhardness of the solution-treated alloy. TEM and SANS analyses revealed that the change in microhardness during aging at 120°C was due to GP zones after 1 h and the coexistence of GP zones, η', and η nanoprecipitates after 1000 h.
3. The addition of P improved both compressive strength and fracture strain of the as-cast alloy due to the refinement of the primary Mg_2Si phase. The solution and peak aging heat treatment also improved the strength and ductility of the alloy by suppressing premature failure and strengthening the Al matrix.

Acknowledgments

This research was supported by National University Development Project at Jeonbuk National University in 2024.

REFERENCES

[1] C. Li, Y.Y. Wu, H. Li, X.F. Liu, Acta Mater. **59**, 1058 (2011).
[2] Q.D. Qin, Y.G. Zhao, C. Liu, P.J. Cong, W. Zhou, J. Alloys Compd. **454**, 142 (2008).
[3] K.K. Ajith Kumar, A. Srinivasan, U.T.S. Pillai, B.C. Pai, M. Chakraborty, Silicon **14**, 9499 (2022).
[4] A.H. Shafieizad, A. Zarei-Hanzaki, H.R. Abedi, K.J. Al-Fadhalah, Mater. Sci. Eng. A **644**, 310–317 (2015).
[5] Q.D. Qin, Y.G. Zhao, W. Zhou, P.J. Cong, Mater. Sci. Eng. A **447**, 186 (2007).
[6] H.Y. Wang, J.N. Zhu, J.H. Li, C. Li, M. Zha, C. Wang, Z.Z. Yang, Q.C. Jiang, CrystEngComm. **19**, 6365 (2017).
[7] N. Soltani, A. Bahrami, M.I. Pech-Canul, Metall. Mater. Trans. A **44**, 4366-4373 (2013).
[8] X.F. Wu, Z.C. Wang, K.Y. Wang, R.D. Zhao, F.F. Wu, J. Alloys Compd. **896**, 163058 (2022).
[9] X. Li, Y. Zhou, D. Yang, J. Wang, M. Li, Z. Wang, X. Tang, H. Zhang, K. Qin, H. Nagaumi, J. Alloys Compd. **1036**, 181688 (2025).
[10] E.-J. Baek, T.-Y. Ahn, J.-G. Jung, J.-M. Lee, Y.-R. Cho, K. Euh, J. Alloys Compd. **696**, 450 (2017).
[11] T.-Y. Ahn, J.-G. Jung, E.-J. Baek, S.S. Hwang, K. Euh, Mater. Sci. Eng. A **695**, 45 (2017).
[12] J.J. Trujillo-Tadeo, J. Victoria-Hernández, P. Garcia-Michelena, P. Jimbert, C. Hartmann, D. Letzig, I. Hurtado, G. Arruebarrena, J. Mater. Res. Technol. **39**, 8602 (2025).
[13] J. Jeon, S.-H. Lee, S. Park, E. Shin, J.-G. Jung, J. Mater. Res. Technol. **41**, 4854-4864 (2026).
[14] S.R. Kline, J. Appl. Crystallogr. **39**, 895-900 (2006).
[15] I. Breßler, J. Kohlbrecher, A.F. Thünemann, J. Appl. Crystallogr. **48**, 1587 (2015).
[16] J. Jeon, S.-H. Lee, S.-D. Kim, Z. Mao, D.N. Seidman, K. Kim, Y.-H. Cho, S.-H. Kim, K. Euh, J.-M. Lee, S.-J. Lee, J.-G. Jung, J. Alloys Compd. **1009**, 177001 (2024).
[17] W. Yang, S. Ji, M. Wang, Z. Li, J. Alloys Compd. **610**, 623 (2014).
[18] X.Z. Li, V. Hansen, J. Gjønnes, L.R. Wallenberg, Acta Mater. **47**, 2651 (1999).
[19] T.-F. Chung, Y.-L. Yang, B.-M. Huang, Z. Shi, J. Lin, T. Ohmura, J.-R. Yang, Acta Mater. **149**, 377 (2018).
[20] C. Li, H.-B. Wei, X.-J. Xu, Q. Zhou, M.-N. Han, S.-H. Sha, Met. Mater. Int. **30**, 857 (2024).
[21] S.-H. Lee, J.-G. Jung, S.-I. Baik, D.N. Seidman, M.-S. Ki, Y.-K. Lee, K. Euh, Mater. Sci. Eng. A **695**, 45 (2017).
[22] A.J. Ardell, Metall. Trans. A. **16**, 2131-2165 (1985).